# A very massive spectroscopic binary in the LH 54 OB association in the LMC

Pablo G. Ostrov⋆

*Facultad de Ciencias Astronómicas y Geofísicas, Paseo del Bosque S/N (1900) La Plata, Argentina*

**ABSTRACT**

We announce the discovery of a new early-type, double-lined spectroscopic binary in the LH 54 OB association in the LMC. We present a $V$ light curve and radial velocities. We investigate the possible configurations of the system, concluding that it probably contains the most massive star measured at the present, with a mass of the order of $100\,\mathrm{M_\odot}$, while its companion has approximately $50\,\mathrm{M_\odot}$.

**Key words:** binaries: eclipsing – stars: early-type – stars: fundamental parameters – stars: individual: LH 54-425

## 1 INTRODUCTION

Though we can trust that the present development of stellar interiors modelling reproduces qualitatively the consecutive stages along the evolution of stars, there still remain appreciable quantitative discrepancies between theoretical predictions and empirical evidence, especiallly in that concern to the higher mass stars. That is not surprising since, on one hand, their modelling is intrinsically more difficult due to their more complex evolution, and on the other hand, very massive stars are rare because of its shorter lifetimes, so that there are scarce observational constraints.

During the last years, we have performed a campaign of observations of early Magellanic stars in order to enrich the empirical knowledge of these objects, particularly in low metallicity regions.

One of the new binaries discovered for which its light curve was completed is a $V \sim 13$ mag star in the LH 54 OB association (Lucke & Hodge 1970). This star ($\alpha = 5^\mathrm{h}26^\mathrm{m}24^\mathrm{s}$, $\delta = -67°30'13''$) is bright enough and has sufficiently big radial velocity excursions to be at scope of the 2.15-m telescope at CASLEO[1] (San Juan, Argentina) for radial velocity measurements.

Hill et al. (1994) identified this object as LH 54-425 and performed $UBV$ photometry, obtaining $V = 13.19 \pm 0.01$, $B - V = -0.31 \pm 0.01$ and $U - B = -1.02 \pm 0.01$. Later on, Oey (1996a) obtained $V = 13.13 \pm 0.007$, $B - V = -0.215 \pm 0.014$ and $U - B = -1.010 \pm 0.015$, listing this star as L54S-4. CCD spectra were also obtained by Oey (1996b)

---

⋆ E-mail: ostrov@fcaglp.edu.ar
[1] Complejo Astronómico El Leoncito, operated under agreement between the Consejo Nacional de Investigaciones Científicas y Técnicas de la República Argentina and the National Universities of La Plata, Córdoba and San Juan.

with the ARGUS multifiber spectrograph at the CTIO 4-m telescope. The spectral type assigned by Oey to this star was O4 III (f⁎). She did not detect double lines at the phase of her observation.

LH 54-425 is the earliest star of the OB association LH 54, located at the East-side of the superbubble DEM 192 (Davies, Elliot & Meaburn 1976) (or N51D, Henize 1956) that is probably related with its growth (Oey & Smedley 1998).

## 2 OBSERVATIONS

LH 54 had been included in one of our selected fields for searching new eclipsing binaries. It was observed during four observing runs between 1998 and 2001.

LH 54-425 showed no eclipses, but exhibited small periodic luminosity changes of the order of $\sim 0.1$ mag, suggesting an ellipsoidal nature of the variability. For this reason we included it as subject for further spectroscopic study as soon as its light curve was sufficiently complete to compute a reasonably reliable ephemeris.

### 2.1 Photometry

CCD images of the region of LH 54 were obtained at CASLEO between 1998 and 2001, with the same instrumentation described in Ostrov et al. (2000). We derived a $V$ light curve from aperture photometry performed with DAOPHOT (Stetson 1987, 1991), and tied all the measurements to a unique instrumental system using several stars as local standards to reduce errors, as described in Ostrov et al. (2000). We performed absolute photometry during a photometric night (Dec 3, 1998), obtaining $V = 13.05 \pm 0.015$, and $B - V = -0.121 \pm 0.011$. Table 1 displays our photometric

measurements of LH 54-425, corrected to the standard system, together with the internal errors derived from the local standards, the $FWHM$ and the airmass for each frame.

## 2.2   Spectroscopy

Spectroscopic observations were obtained by means of a RE-OSC spectrograph in its single dispersion mode, attached to the 2.15-m telescope at CASLEO. The CCD detector was the same Tektronik used for photometry. We used a 600 mm$^{-1}$ grating giving a reciprocal dispersion of 1.63 Å/pixel on the range from 3900 to 5500 Å. Our resolution, measured from the Cu-Ne-Ar comparison lamp lines, was 2 pixels.

We obtained spectra near the quadratures in series of three 1200 s exposures. The spectrograms were processed and extracted using IRAF[2] routines. Each series of three observations was combined in one spectrogram, before performing the concomitant measurements.

## 3   ANALYSIS

### 3.1   Ephemeris

We applied to the photometric data two period search methods: one derived from the Lafler & Kinman's (Lafler & Kinman 1965) and the one described in Shwarzenberg-Czerny (1997). Because of our short time base and the intrinsically small light variations, we can not derive a precise ephemeris. We found that the most probable period is $P = 2.2475$ days, with aliases each 0.007 days. We used this period and $E_0 = 2452216.597$ to plan the spectroscopic observations.

### 3.2   Spectroscopic classification

We classified the spectra following the criteria of Walborn & Fitzpatrick (1990). The earliest component shows no lines of He I, corresponding thus an O3 spectral type. The other component shows He I 4471 hardly visible due our poor signal to noise ratio (in fact, it is only detectable in our best spectrograms, obtained during dark nights) and more intense He II lines which is in agreement with an approximately O5 type. With regard to the luminosity classes, we combined all the spectrograms acquired in each quadrature to increment the signal to noise ratio. In the averaged spectrograms, N IV 4058 emission from the primary is visible, together with Si IV $\lambda\lambda$ 4089 or 4116 depending on the phase (this is alternatively blended with the H$\delta$ absorption of the secondary). We are not able to assign a luminosity class to the secondary. So, we classify the system as O3 III(f*)+O5:. Fig. 1 shows the CCD spectrograms of LH 54-425 obtained during dark nights, corresponding to both quadratures.

### 3.3   Radial velocity measurements

The He II 4686 line appears clearly double in all our spectrograms. He II 4200 and He II 4542 appear double in some

---

[2]   IRAF software is distributed by NOAO, operated by AURA for NSF.

**Table 2.** Radial velocities

| HJD-2450000 | phase | Primary [km s$^{-1}$] | Secondary [km s$^{-1}$] | [O III] [km s$^{-1}$] |
|---|---|---|---|---|
| 2286.732 | 0.702 | 122 | 679 | 286 |
| 2287.721 | 0.146 | 500 | 19 | 286 |
| 2329.516 | 0.742 | 114 | 704 | 269 |
| 2330.537 | 0.197 | 496 | -169 | 280 |
| 2330.645 | 0.245 | 450 | -119 | 280 |
| 2331.546 | 0.646 | 96 | 648 | 284 |

spectrograms and severely blended in others. The He II absorption pairs were measured by means of a double gaussian fit using the "deblend" function of the "splot" IRAF task. Only the easily separable He II pairs were used for the radial velocity determinations. Table 3.3 lists the heliocentric radial velocities derived for both binary components, together with that corresponding to the nebular [O III]$\lambda$ 5007 emission, used to check the stability of the system.

### 3.4   Geometry system's exploration

Since the system shows no true eclipses, it is not possible to derive reliable physical parameters just from the light curve and radial velocities. For this reason, we assumed an absolute magnitude and investigate which system configurations were compatible with the observations.

We computed the models with the Wilson-Devinney codes (Wilson 1990, Wilson & Devinney 1971). For the bolometric albedos and gravity darkening coefficients we assumed values of $A = 1.0$ and $g = 1.0$, respectively, which are adequate for radiative envelopes (Rucinski 1969, Lucy 1976). For the limb darkening a square root law (Díaz-Cordovés & Giménez, 1992) was used, taking the corresponding coefficients from tables by Díaz-Cordovés et al. (1995).

#### 3.4.1   Detached configurations

We first explored the possible detached configurations, so the mode of operation 2 of the Wilson-Devinney program was chosen. In order to reduce the degrees of freedom of the problem, we fixed the total bolometric magnitude of the system. We considered three cases, with $M_{bol} = -10, -10.3$ and $-10.6$. For the models with $M_{bol} = -10$ we assigned temperatures of 52500 K and 44500 K, corresponding to spectral types O3 V and O5 V according with Schmidt-Kaler (1982), while for those models with $M_{bol} = -10.6$ we adopted the temperature scale of Chlebowski & Garmany (1991) for O3 III and O5 III stars, 46500 K and 42300, respectively. For the models with intermediate bolometric magnitude we used the mean of the two temperature scales. With this procedure, the extreme cases in distance moduli and temperature scales were considered.

For each adopted orbital inclination, temperatures and potential $\Omega_1$ of the primary, the secondary's potential $\Omega_2$ was chosen according with the assumed total bolometric magnitude of the system.

Fig. 2 displays the results of the experiments with detached configurations. Points of bigger size represent smaller O-C light curve residuals. The lower limit corresponds to the primary being 2.5 magnitudes brighter than the secondary

**Table 1.** *V* light photometry of LH 54-425

| HJD 2450000+ | V | $\sigma_i$ | fwhm " | X | HJD 2450000+ | V | $\sigma_i$ | fwhm " | X |
|---|---|---|---|---|---|---|---|---|---|
| 1149.807 | 13.087 | 0.011 | 2.09 | 1.30 | 1503.601 | 13.048 | 0.008 | 2.62 | 1.48 |
| 1149.834 | 13.061 | 0.011 | 2.36 | 1.36 | 1503.687 | 13.058 | 0.006 | 2.86 | 1.27 |
| 1150.847 | 13.082 | 0.012 | 1.91 | 1.40 | 1503.742 | 13.059 | 0.007 | 2.40 | 1.23 |
| 1151.617 | 13.067 | 0.006 | 1.92 | 1.33 | 1503.795 | 13.069 | 0.005 | 2.84 | 1.25 |
| 1151.671 | 13.059 | 0.008 | 2.04 | 1.25 | 1503.836 | 13.069 | 0.004 | 2.83 | 1.30 |
| 1151.731 | 13.050 | 0.004 | 2.00 | 1.23 | 1504.575 | 13.048 | 0.006 | 3.46 | 1.58 |
| 1151.786 | 13.056 | 0.006 | 2.13 | 1.28 | 1504.628 | 13.046 | 0.007 | 3.14 | 1.39 |
| 1151.857 | 13.048 | 0.006 | 2.05 | 1.44 | 1504.736 | 13.050 | 0.008 | 3.49 | 1.23 |
| 1152.663 | 13.085 | 0.005 | 2.26 | 1.26 | 1504.776 | 13.051 | 0.007 | 2.72 | 1.24 |
| 1152.709 | 13.076 | 0.007 | 1.98 | 1.23 | 1504.814 | 13.053 | 0.006 | 3.00 | 1.27 |
| 1152.751 | 13.073 | 0.005 | 2.19 | 1.24 | 1504.842 | 13.060 | 0.007 | 3.16 | 1.32 |
| 1152.800 | 13.066 | 0.006 | 1.98 | 1.31 | 1859.592 | 13.058 | 0.007 | 3.62 | 1.63 |
| 1152.831 | 13.062 | 0.006 | 1.86 | 1.37 | 1859.615 | 13.059 | 0.005 | 3.18 | 1.53 |
| 1153.692 | 13.105 | 0.007 | 1.62 | 1.23 | 1859.652 | 13.052 | 0.006 | 3.04 | 1.40 |
| 1153.735 | 13.106 | 0.006 | 1.76 | 1.24 | 1859.683 | 13.052 | 0.004 | 3.51 | 1.32 |
| 1153.768 | 13.092 | 0.006 | 1.87 | 1.26 | 1859.709 | 13.054 | 0.005 | 4.02 | 1.28 |
| 1153.823 | 13.079 | 0.005 | 2.36 | 1.36 | 1859.721 | 13.045 | 0.019 | 6.23 | 1.26 |
| 1153.857 | 13.070 | 0.008 | 2.40 | 1.46 | 1859.763 | 13.063 | 0.013 | 6.23 | 1.23 |
| 1154.706 | 13.110 | 0.005 | 2.06 | 1.23 | 1859.806 | 13.046 | 0.004 | 5.11 | 1.24 |
| 1154.740 | 13.100 | 0.005 | 2.16 | 1.24 | 1859.838 | 13.047 | 0.007 | 4.63 | 1.26 |
| 1154.804 | 13.102 | 0.007 | 2.48 | 1.32 | 1860.592 | 13.092 | 0.010 | 5.08 | 1.62 |
| 1154.845 | 13.096 | 0.004 | 2.45 | 1.43 | 1860.687 | 13.073 | 0.006 | 5.37 | 1.31 |
| 1155.674 | 13.105 | 0.005 | 2.03 | 1.24 | 1860.760 | 13.065 | 0.005 | 3.87 | 1.23 |
| 1155.712 | 13.111 | 0.004 | 1.99 | 1.23 | 1860.832 | 13.070 | 0.006 | 5.22 | 1.26 |
| 1155.748 | 13.115 | 0.005 | 2.05 | 1.25 | 1860.867 | 13.053 | 0.005 | 4.74 | 1.31 |
| 1155.776 | 13.116 | 0.005 | 1.86 | 1.28 | 1861.604 | 13.109 | 0.007 | 3.65 | 1.55 |
| 1155.826 | 13.115 | 0.007 | 2.49 | 1.38 | 1861.733 | 13.092 | 0.005 | 4.05 | 1.25 |
| 1155.851 | 13.108 | 0.006 | 2.56 | 1.45 | 1861.815 | 13.075 | 0.004 | 3.37 | 1.25 |
| 1499.825 | 13.090 | 0.004 | 2.90 | 1.27 | 1861.860 | 13.067 | 0.006 | 3.66 | 1.31 |
| 1500.589 | 13.089 | 0.011 | 3.61 | 1.56 | 1862.572 | 13.112 | 0.007 | 3.65 | 1.69 |
| 1500.659 | 13.101 | 0.004 | 2.89 | 1.34 | 1862.638 | 13.109 | 0.006 | 3.44 | 1.42 |
| 1500.732 | 13.107 | 0.004 | 3.01 | 1.24 | 1862.698 | 13.109 | 0.006 | 3.26 | 1.28 |
| 1500.799 | 13.110 | 0.007 | 3.19 | 1.24 | 1862.751 | 13.099 | 0.005 | 3.36 | 1.23 |
| 1500.844 | 13.104 | 0.006 | 3.34 | 1.30 | 1862.833 | 13.092 | 0.005 | 3.53 | 1.27 |
| 1501.549 | 13.068 | 0.005 | 3.30 | 1.76 | 1863.564 | 13.104 | 0.005 | 2.64 | 1.72 |
| 1501.593 | 13.077 | 0.007 | 3.38 | 1.53 | 1863.634 | 13.117 | 0.007 | 3.08 | 1.42 |
| 1501.616 | 13.079 | 0.007 | 3.25 | 1.45 | 1863.720 | 13.118 | 0.004 | 2.69 | 1.25 |
| 1501.677 | 13.090 | 0.004 | 3.10 | 1.30 | 1863.810 | 13.116 | 0.004 | 3.45 | 1.25 |
| 1501.756 | 13.098 | 0.005 | 2.60 | 1.23 | 1864.619 | 13.084 | 0.006 | 2.27 | 1.46 |
| 1501.815 | 13.106 | 0.004 | 3.00 | 1.26 | 1864.681 | 13.093 | 0.006 | 1.79 | 1.30 |
| 1502.565 | 13.047 | 0.008 | 3.93 | 1.65 | 1864.755 | 13.108 | 0.005 | 2.38 | 1.23 |
| 1502.699 | 13.078 | 0.009 | 2.36 | 1.26 | 1864.812 | 13.119 | 0.006 | 2.80 | 1.25 |
| 1502.784 | 13.083 | 0.008 | 2.12 | 1.24 | 2212.865 | 13.071 | 0.006 | 2.82 | 1.26 |
| 1502.832 | 13.089 | 0.008 | 2.14 | 1.29 | 2213.797 | 13.060 | 0.005 | 2.74 | 1.23 |
| 1502.861 | 13.096 | 0.018 | 3.99 | 1.34 | 2214.855 | 13.062 | 0.006 | 1.99 | 1.25 |

component, which can be rejected according to the relative intensity of the corresponding spectral lines. The upper limit corresponds to semi-detached configurations, with the secondary star filling its Roche-lobe. Models above the solid curve have the secondary brighter than the primary, therefore can be also disregarded.

The upper panel, that corresponds to highest temperatures and lower luminosity, shows that the best fitting models are near the semi-detached configuration, with the secondary filling its Roche-lobe. These models are not realistic from an evolutionary perspective, since they have secondary components of bigger size than the primary. If the less massive star is the more evolved one, we have to conclude that

mass inversion has occurred, and the system is now semi-detached.

In the middle panel we considered models with intermediate luminosities and temperatures. The best solutions are aligned at the upper limit of the models considered, indicating a semi-detached configuration. There are also good models with $i \sim 58 \deg$ and $\Omega_1 \sim 3$. It means that the *primary* star is almost filling its Roche-lobe. However, it is not very plausible since the magnitude difference between both
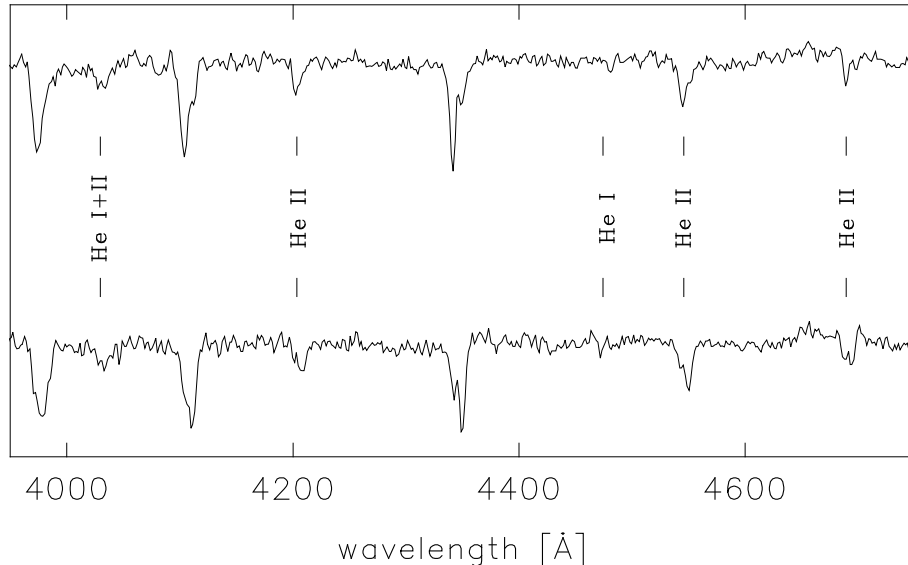
**Figure 1.** CCD spectra of LH 54-425 obtained at CASLEO, corresponding to both quadratures.

stars is near 2.5 mag, which does not agree with the spectroscopic evidence [3].

The residuals from models with lowest temperature scale and highest total luminosity (which allows the biggest sizes of the stars) are presented in the bottom panel. In this case, besides of the semi-detached configurations, there exist plausible detached solutions, with $i \sim 47$ deg. The lowest value considered for the potential $\Omega_1$ (2.85) implies that the primary component is almost filling its Roche-lobe, although (as mentioned above) in these models the luminosity difference between both stars is excessive.

### 3.4.2   Semi-detached configurations

Considering that some results of the experiments suggested that the system is semi-detached, with the cooler and less massive star filling its Roche-lobe, we explored these configurations, using therefore the mode of operation 5 in the Wilson-Devinney programs. Figure 3 shows the residuals of these models, corresponding to the high and low temperature scales above mentioned, respectively. As the margins of plausible models are wide, it is necessary to consider limits to the total luminosity to restrict the amount of solutions. The upper and bottom curves drawn on figure 3 correspond to models with $M_{bol} = -10$ and $M_{bol} = -10.6$, respectively, while models above the horizontal line have the secondary more luminous than the primary component. Configurations with $\Omega_1$ smaller than those plotted in the graphics are in overcontact, and can be also rejected according to the assumed limits in the total luminosity of the system.

---

[3]  It does not allows to disregard completely such solutions. For example, Niemelä & Bassino (1994) called "primary" at the Roche-lobe filling component of HV 2543, based on the intensity of their spectral lines, while from the W-D modelling that star is approximately 0.9 $V$ magnitudes fainter than its companion.

## 4   RESULTS

In spite of the wide range of models that can fit well the observations, we can state with reasonable confidence that the inclination is roughly $45 \sim 50°$, since bigger values would cause eclipses. This implies that the masses are $\sim 100$ and $\sim 50 M_\odot$ for the O3 and the O5 component, respectively. Table 4 summarises the parameters that best fit suitable detached and semi-detached solutions. It must be noted that the errors quoted in Table 4 correspond to fixed values of $i$, $\Omega_1$ and $\Omega_2$, i.e., the errors of the masses reflect only the errors in the radial velocity measurements.

The modelled light and radial velocity curves are displayed in Fig. 4 and Fig. 5, together with the observations and O-C residuals. The models correspond to the best fitting detached configuration, although there are not visible difference with the best fitting semi-detached solution.

In the more modest case, the inclination is $i \sim 58°$ and the corresponding masses are $\sim 64$ and $\sim 31 M_\odot$, although this model have a primary 2.3 magnitudes brighter than the secondary component, that is not supported by the spectroscopic data. (The other extreme case, in that both stars have similar brightness, corresponds to $i \sim 39°$ and gives masses of $\sim 160$ and $\sim 80 M_\odot$). All possible solutions indicate that this system contains the more massive star measured at the present.

In a previous work (Ostrov 2001) we found from the analysis of another early Magellanic binary with O3If* and O6V components, masses of 41 and 27 $M_\odot$. That was an overcontact system, with a still shorter period, of only 1.4 days. These results suggests that extremely early stars have a wide range of masses, at least when they belong to very close binaries, where mass exchange and mass loss play a fundamental role in the evolution.

Indeed, observations of these systems with higher signal to noise and dispersion than that reachable at CASLEO would provide valuable data to investigate the similitudes and differences between these objects.
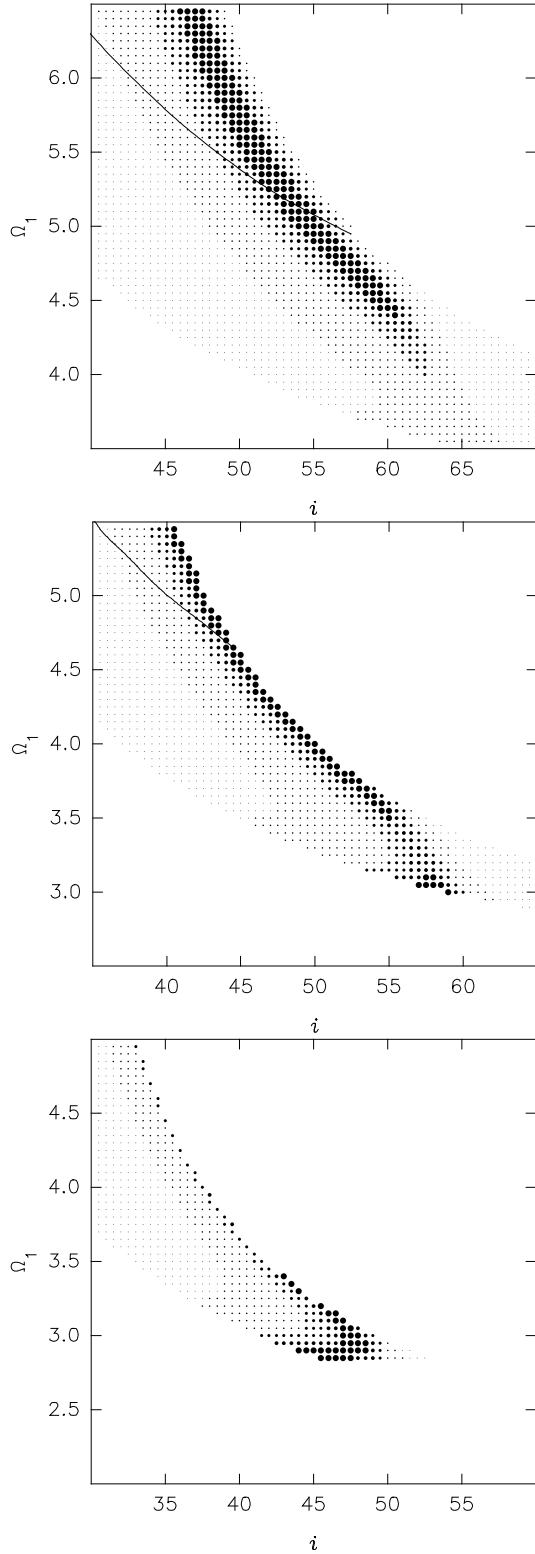
**Figure 2.** Residuals of the detached models. Points of different sizes represent the sums of squared residuals, the bigger symbols corresponding to the smaller amounts. The limits between different point sizes are 1.65, 3.30, 4.95 and 8.24 times the sum of squared residuals of the best fitting model. The different panels correspond to different assumed effective temperatures and total luminosity of the system, as quoted in the text.
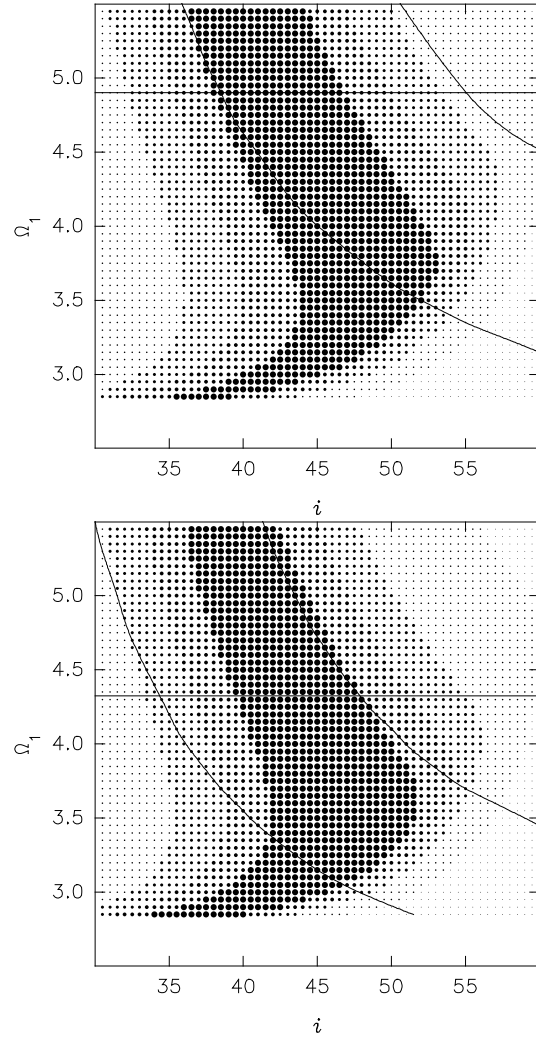


**Figure 3.** Residuals of the semi-detached models. Points of different sizes represent the sums of squared residuals, as in Fig. 2. Top and bottom panels correspond to different assumed temperature scales, as quoted in the text.

### ACKNOWLEDGMENTS

### REFERENCES

Chlebowski T., Garmany D., 1991, ApJ 368, 241
Davies R.D., Elliot K.H., Meaburn J., 1976, Mem. R. Astron. Soc. 81, 89
Díaz-Cordovés, J., Giménez, A. A&A, 259, 227
Díaz-Cordovés, J., Claret, A., Giménez, A., A&AS, 110, 329
Henize K.G., 1956, ApJS, 2, 315
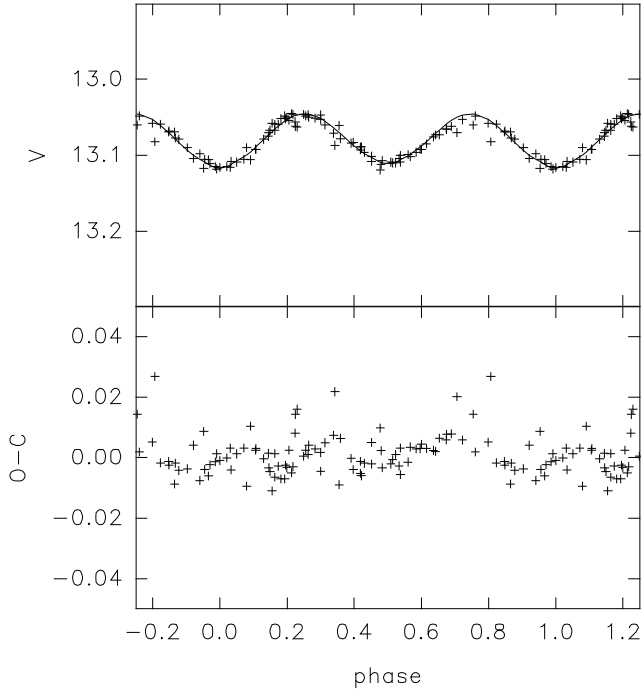
**Figure 4.** The observed and modelled *V* light curve for LH 54-425 and their concomitant O-C residuals.

Hill R.J., Madore B.F., Freedman W.L., 1994, ApJS 91, 538
Lafler J., Kinman T.D., 1965, ApJS 11, 216
Lucke P.B., Hodge P.W., 1970, AJ, 75, 171
Lucy L.B., 1976, ApJ 205, 208
Niemelä V.S., Bassino L.P., 1994, ApJ 437, 332
Oey M.S., Smedley S.A., 1998, AJ, 116, 1263
Oey M.S., 1996a, ApJS, 104, 71
Oey M.S., 1996b, ApJ, 465, 231
Ostrov P.G., 2001, MNRAS 321, L25
Ostrov P.G., Lapasset E., Morrell N.I., 2000, A&A 356, 935
Rucinski S.M., 1969, Acta Astron. 19, 245
Schmidt-Kaler, Th., 1982, In: Landolt-Börnstein, New Series, ed.
    K. Shaifers & H.H. Voigt, Group VI, Vol. 2/b
Shwarzenberg-Czerny A., 1997, ApJ 489, 941
Stetson P.B., 1987, PASP 99, 191
Stetson P.B., 1991, In: Grosbøl P.J., Warmel R.H. (eds.) 3rd
    ESO/ST-ECF Data Analysis Workshop, p. 187
Vacca W.D., Garmany C.D., Shull J.M, 1996, ApJ 460, 914
Walborn N.R., Fitzpatrick E.L., 1990, PASP 102, 650
Wilson R.E., 1990, ApJ 356, 613
Wilson R.E., Devinney E.J., 1971, ApJ 166, 605
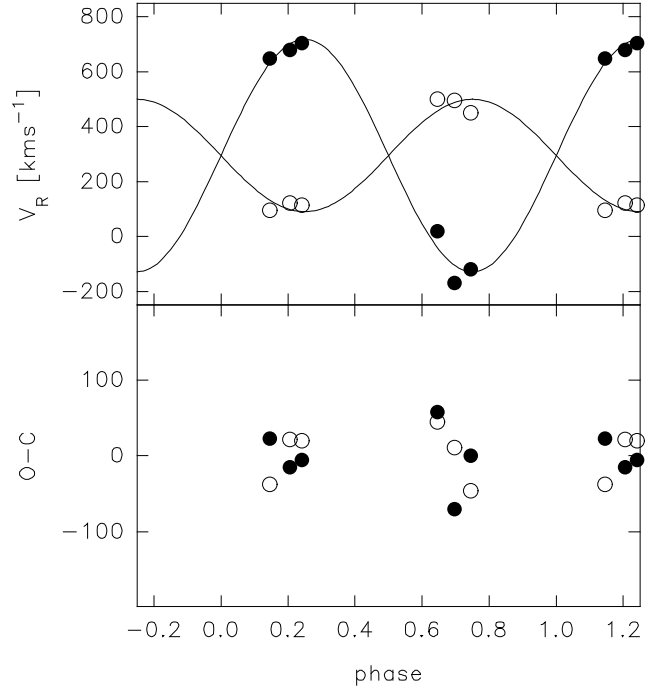
**Figure 5.** Observed and modelled radial velocity curve for LH 54-425 and their O-C residuals. Hollow circles correspond to the primary component and filled ones stand for the secondary.

**Table 3.** Best fitting plausible models

| | Adopted Values | |
|---|---|---|
| $T_1$ | | 46500 K |
| $T_2$ | | 42300 K |
| $M_{bol}$ | | −10.6 |
| | Fitted Values | |
| $V_\gamma$ | | $295.0 \pm 3 \, \mathrm{km \, s^{-1}}$ |
| $q \, (M_2/M_1)$ | | $0.48 \pm 0.01$ |
| configuration | detached | semi-detached |
| $i$ (adopted) | 47° | 45.5° |
| $\Omega_1$ (adopted) | 3.1 | 3.15 |
| $\Omega_2$ | 2.86[a] | 2.84[b] |
| $a$ | $38.1 \pm 0.4 \, \mathrm{R_\odot}$ | $39.3 \pm 0.4 \, \mathrm{R_\odot}$ |
| $\Sigma res^2$ | 0.0033222 | 0.0033563 |
| | Star Dimensions | |
| $M_1$ | $100 \pm 3 \, \mathrm{M_\odot}$ | $108 \pm 3 \, \mathrm{M_\odot}$ |
| $R_1$ | $15.1 \, \mathrm{R_\odot}$ | $15.1 \, \mathrm{R_\odot}$ |
| $M_{\mathrm{bol} \, 1}$ | −10.2 | −10.2 |
| $\log g_1 [cgs]$ | $4.1 \pm 0.1$ | $4.1 \pm 0.1$ |
| $M_2$ | $48.4 \pm 3 \, \mathrm{M_\odot}$ | $52.2 \pm 3 \, \mathrm{M_\odot}$ |
| $R_2$ | $11.9 \, \mathrm{R_\odot}$ | $12.4 \, \mathrm{R_\odot}$ |
| $M_{\mathrm{bol} \, 2}$ | −9.3 | −9.3 |
| $\log g_2 [cgs]$ | $4.0 \pm 0.1$ | $4.0 \pm 0.1$ |

[a] Chosen according the total luminosity of the system.

[b] $\Omega_{\mathrm{crit}}$